J Mater Sci (2009) 44:198–203
DOI 10.1007/s10853-008-3104-1

A simple gel route to synthesize nano-$Li_4Ti_5O_{12}$ as a high-performance anode material for Li-ion batteries

D. Wang · N. Ding · X. H. Song · C. H. Chen

Received: 5 July 2008 / Accepted: 4 November 2008 / Published online: 27 November 2008

Abstract Nano-$Li_4Ti_5O_{12}$ powders were synthesized by a simple gel route with acrylic acid, tetrabutyl titanate, and lithium nitrate as the precursors that were made into gels through thermal polymerization. The $Li_4Ti_5O_{12}$ powders were obtained by calcination of the gels at 700, 750, and 800 °C. They were characterized by thermal gravimetric analysis, differential thermal analysis, X-ray diffraction, and field emission scanning electron microscopy. The electrochemical performance of these nano-$Li_4Ti_5O_{12}$ powders was examined with galvanostatic cell cycling. The average particle size of the 700-, 750-, and 800 °C-calcined powders is about 70, 120, and 400 nm, respectively. The 750 °C-calcined powder exhibits a high capacity of over 160 mAh/g after 100 cycles and a good rate capability with a capacity of 122 mAh/g even at 10C rate.

Introduction

Recently, spinel-type $Li_4Ti_5O_{12}$ as anode material for Li-ion batteries has attracted more and more attentions [1–8], owing largely to its great merit of zero-strain characteristic during lithium insertion/extraction when compared with other anode materials [9]. Because the mechanical failure coming from the volume change during electrochemical cycling is usually the main reason for capacity fading in the Li-ion batteries application, this unique feature of $Li_4Ti_5O_{12}$ allows it with a very long cycle life. Also, the voltage profile of $Li_4Ti_5O_{12}$ exhibits a very flat plateau at 1.55 V vs. Li^+/Li that is more stable compared with the highly reducing metallic lithium or lithiated carbon materials [9]. Hence, such a 1.55 V flat plateau makes $Li_4Ti_5O_{12}$ to be a safe anode material when coupled with a high potential cathode material such as $LiMn_2O_4$ or $LiNi_{0.5}Mn_{1.5}O_4$ in industrial applications [4, 10]. On the other hand, $Li_4Ti_5O_{12}$ is a poor electrical conductor with a conductivity of only 10^{-13} S/cm at room temperature [6]. Therefore, the preparation of submicron or even nanosized $Li_4Ti_5O_{12}$ powders becomes necessary so that the diffusion length of lithium can be largely shortened.

In previous studies, $Li_4Ti_5O_{12}$ has been mostly synthesized by solid state reaction [6, 9, 11–14] and sol–gel methods [15–19]. Inspite of its convenience for a large-scale production, the solid state reaction process usually cannot produce the powders with the particle size in the nanometer scale, which may strongly affect their electrochemical performance. The particle size of powders prepared by the sol–gel method can reach sub-micron scale, but the synthesis process is usually difficult to control and time consuming. Herein, we describe a simple gel method to synthesize nano-$Li_4Ti_5O_{12}$ by means of thermal polymerization of a mixture of acrylic acid, tetrabutyl titanate, and lithium nitrate followed by a heat treatment procedure at elevated temperatures. The $Li_4Ti_5O_{12}$ powders obtained under optimized conditions show excellent electrochemical performance.

Experimental

The stoichiometric amounts of lithium nitrate ($LiNO_3$) and tetrabutyl titanate ($Ti(OC_4H_9)_4$) with a Li:Ti molar ratio of 4:5 were weighed separately. Then $Ti(OC_4H_9)_4$ was

D. Wang · N. Ding · X. H. Song · C. H. Chen (✉)
Department of Materials Science and Engineering, University of Science and Technology of China, Anhui Hefei 230026, China
e-mail: cchchen@ustc.edu.cn

dissolved in acrylic acid (AA) with Ti:AA molar ratio of 1:20 (solution A). $LiNO_3$ was dissolved in a mixture of distilled water and nitric acid (65%) with H_2O:HNO_3 = 7:2 (v/v) to obtain a concentration of 0.15 M (solution B). Subsequently, the solution B was added to the solution A with continuous magnetic stirring for 30 min to obtain a clear light yellowish solution. Note that nitric acid was used here to restrain the hydrolysis of $Ti(OC_4H_9)_4$. Then the mixed solution was placed in an oven and kept at 150 °C for 15 h. At this temperature, acrylic acid should undergo a polymerization process to form poly(acrylic acid) [20]. It was observed that the clear solution was boiled for the first 1 h. It became translucent and milky white along with the simultaneous evaporation of AA. Finally, a brown homogeneous dry gel was obtained. In order to determine a proper temperature range for the heat treatment of the gel, thermal gravimetric analysis (TGA) and differential thermal analysis (DTA) of the dry gel were conducted in air at a heating rate of 10 °C/min using a thermal analyzer (Shimadzu DT-50). The proper calcination temperatures were found to be 700–800 °C (see below). Hence, the dry gel was calcined at 700, 750, and 800 °C, respectively, in air for 12 h to obtain three kinds of powders.

The crystal structure of these powders was characterized by X-ray diffraction (XRD) using a diffractometer (Philips X'Pert Pro Super, Cu Kα radiation). The diffraction patterns were recorded at room temperature in the 2θ range from 10 to 80°. The particle morphology of the powders was observed by a field emission scanning electron microscope (FESEM LEO 1530). They were also measured with a surface area analyzer (SA 3100) to obtain their BET-specific surface area.

The electrochemical properties of the synthesized $Li_4Ti_5O_{12}$ powders were analyzed with $Li_4Ti_5O_{12}$/Li half cells. The working electrode consisted of a mixture of 80 wt% $Li_4Ti_5O_{12}$, 10 wt% carbon black, and 10 wt% polyvinylidene fluoride (PVDF) binder. The weight of active material ($Li_4Ti_5O_{12}$) was roughly 6–7 mg per electrode. The counter electrode was metallic lithium, and the electrolyte was 1 M $LiPF_6$ in EC/DEC (1:1). Coin cells (CR2032 size) were assembled in an argon-filled dry-box. Electrochemical tests were carried out on a multi-channel battery test system (NEWARE BTS-610) in the galvanostatic charge–discharge mode in the voltage range from 1.0 to 2.5 V. The current was set from 0.1 to 10 mA. The direct current (DC) resistance of the cells in the 8th cycle was measured by the intermittent current interruption method at the current of 0.31 mA (0.2 mA/cm^2). During the discharge process, a 60 s current interruption was performed every 5 min to obtain the cell resistance at various states of discharge. By repeating the above steps, the curves of the cell resistance vs. discharge capacity were obtained.

Results and discussions

Figure 1 presents the TG–DTA curves of the dry gel which contains poly(acrylic acid) (PAA) and Li–Ti precursor compounds. Three distinct steps of weight loss can be distinguished on the TG–DTA curves. At the first step (20–200 °C), a very small weight loss (less than 3%) is observed, which can be attributed to the vaporization of both adsorbed and residual water in the gel. At the second step (200–500 °C), a series of exothermic processes take place, when especially a strong exothermic peak at 486 °C is detected. These processes should be due to the vigorous combustion reactions between the organic components (such as PAA) and nitrate components (such as $LiNO_3$) or air. At the same time, these processes are accompanied with a huge weight loss of about 90% in total due to the evolution of NO_2, CO_2, and H_2O resulting from the decomposition of nitrate and the combustion of PAA. At the third step above 500 °C, no weight loss and no obvious thermal effect are observed, except that a slow exothermic process seems to occur. This slight exothermic process might be due to the crystallization of $Li_4Ti_5O_{12}$ particles.

Because a powder calcined at 650 °C gives rise to a poor electrochemical property (not shown here), three different calcination temperatures 700, 750, and 800 °C were used to achieve better crystallization. Figure 2 shows the X-ray diffraction patterns of the powders calcined at these temperatures. The sample calcined at 700 °C is composed of spinel $Li_4Ti_5O_{12}$ as the main phase together with rutile TiO_2 and anatase TiO_2 as impurity phases. At 750 °C, the peaks of anatase TiO_2 disappear due probably to the phase transition from anatase to rutile. The rutile TiO_2 phase is still present even when the calcination temperature is up to 800 °C. In fact, there is no obvious

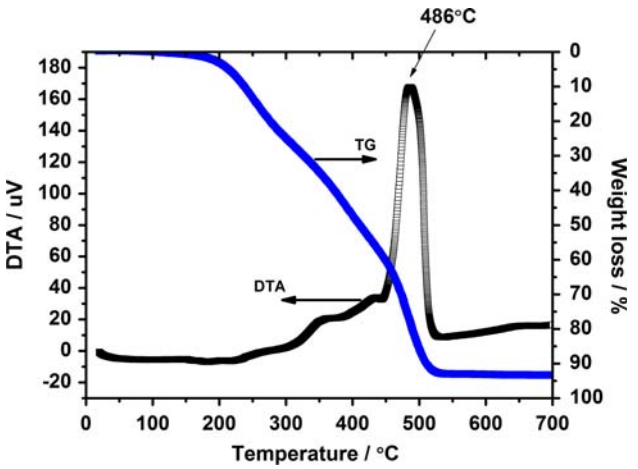

Fig. 1 TG–DTA curves of the dry gel which contains poly(acrylic acid) and Li–Ti precursor compounds. The heating rate was 10 °C/min

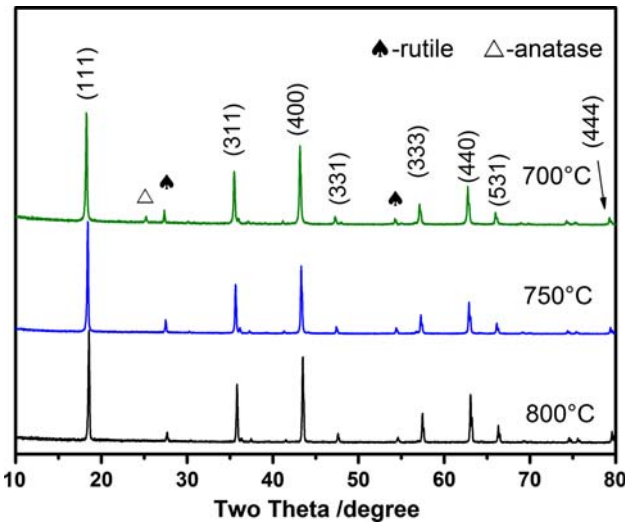

Fig. 2 X-ray diffraction patterns of $Li_4Ti_5O_{12}$ powders calcined at different temperatures

difference in the diffraction patterns of the samples calcined between 750 and 800 °C.

Figure 3 shows the FESEM micrographs of the powders calcined at different temperatures. Obviously, the particle size increases gradually with calcination temperature. The average particle size of the powder calcined at 700 °C is 70 nm with a distribution of 60–80 nm, compared to 120 nm with a distribution of 50–200 nm for the 750 °C-calcined one and 400 nm with a distribution of 80–500 nm for the 800 °C-calcined one. Thus, the formation of nanosized particles by this gel-route method is realized by the combustion of the gel at relatively low temperatures. In the gelation process, the viscous polymerizing mixture of AA and PAA as the dispersion medium can suppress the agglomeration of the TiO_2 particles freshly generated from $Ti(OC_4H_9)_4$ and enhance the homogenous mixing of lithium ions and the TiO_2 particles. Furthermore, the combustion of PAA precursor and the decomposition of the nitrate precursor should produce a large amount of heat, which can make the nucleation process of $Li_4Ti_5O_{12}$ grains to be completed at a relatively low temperature, and the accompanying gas evolution can prevent the particles from agglomerating and growing up. This may explain why the nano-$Li_4Ti_5O_{12}$ can be obtained at the relatively low temperatures by our method.

The BET surface areas of the powders are measured to be 5.8 m^2/g (700 °C), 1.3 m^2/g (750 °C), 1.0 m^2/g (800 °C), respectively. These values are substantially smaller than those estimated from the particle sizes observed by FESEM (Fig. 3). Obviously, the agglomeration of the particles in these powders can explain such a difference.

Figure 4 shows the initial charge–discharge curves the $Li_4Ti_5O_{12}$/Li cells at a constant current of 0.31 mA.

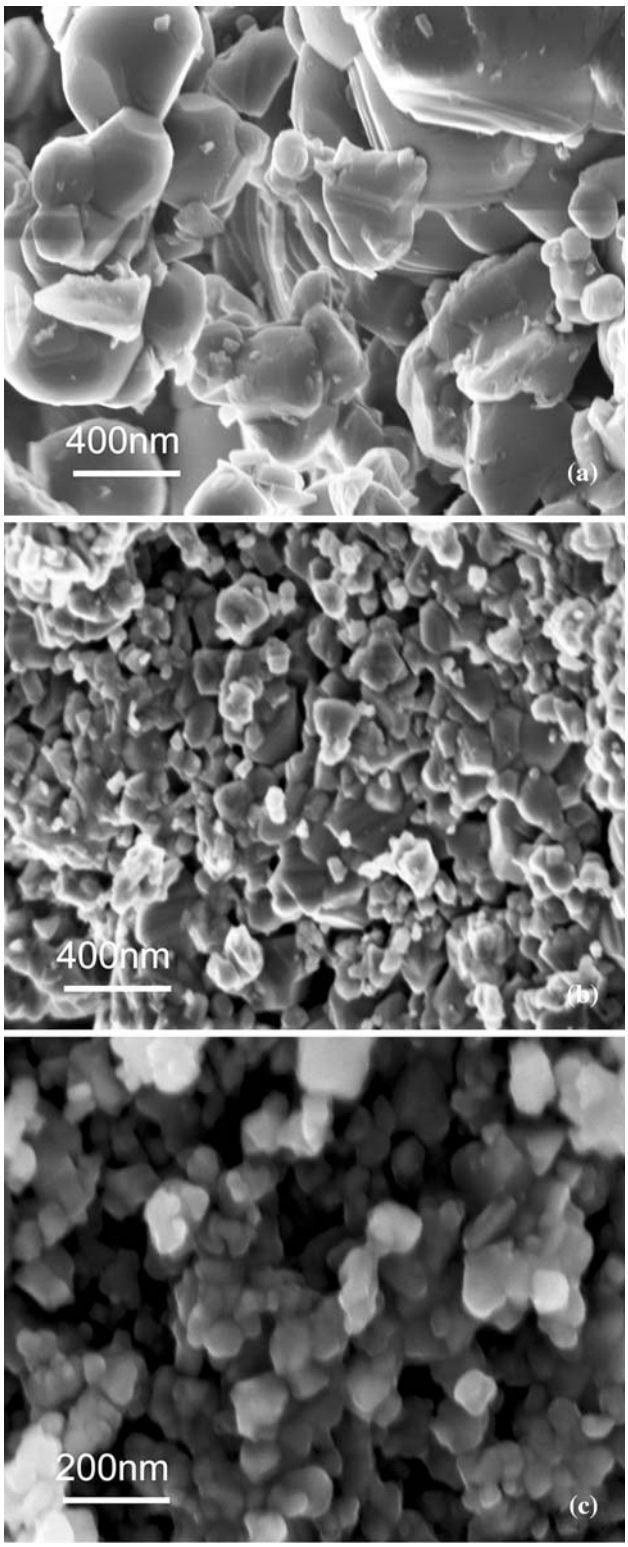

Fig. 3 FESEM images of $Li_4Ti_5O_{12}$ powders calcined at different temperatures: **a** 800 °C, **b** 750 °C, and **c** 700 °C

The charge–discharge curves show very flat plateaus at the potential of around 1.55 V vs. Li^+/Li, which indicates that it is a two-phase reaction: $Li_4Ti_5O_{12} + 3Li \underset{\text{charge}}{\overset{\text{discharge}}{\Leftrightarrow}} Li_7Ti_5O_{12}$

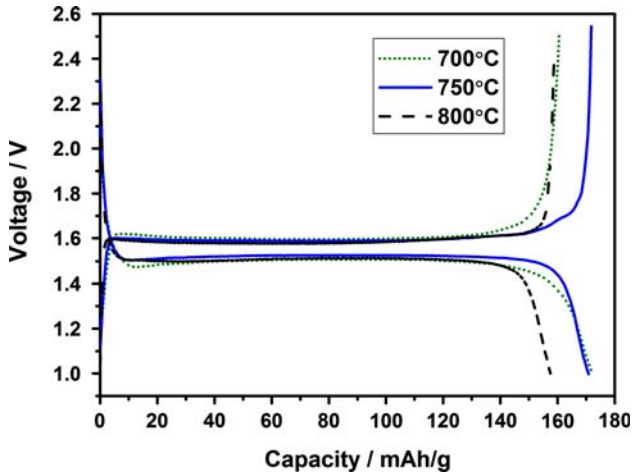

Fig. 4 Initial charge–discharge curves of the $Li_4Ti_5O_{12}$/Li cells at constant current of 0.31 mA

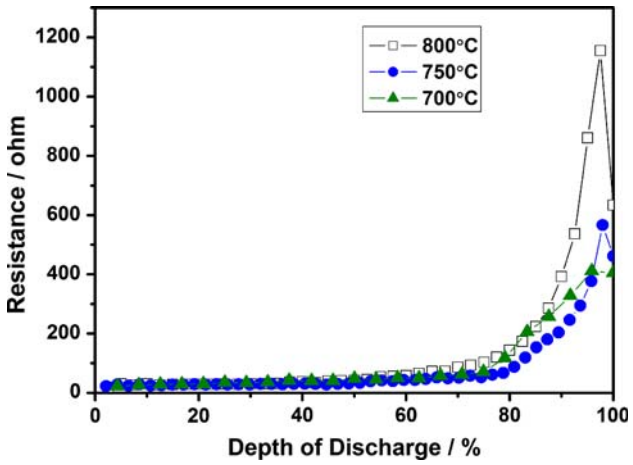

Fig. 6 Direct current resistance (60 s current interruption) of the $Li_4Ti_5O_{12}$/Li cells as a function of depth of discharge for the $Li_4Ti_5O_{12}$ powders calcined at various temperatures

[9]. The discharge capacity of $Li_4Ti_5O_{12}$ (700 °C) is 171 mAh/g, while that of $Li_4Ti_5O_{12}$ (750 °C) is 170 mAh/g, both of which are very close to the theoretical capacity of 175 mAh/g calculated by $C = \frac{96500 \times n}{3.6 \times M}$, where n is the number of active lithium involved in 1 mol of $Li_4Ti_5O_{12}$, and M is its molecular weight. In comparison, the initial discharge capacity of $Li_4Ti_5O_{12}$ (800 °C) is only 158 mAh/g. This low capacity is likely due to its larger particle size, which increases the diffusion lengths from the surface to the core of $Li_4Ti_5O_{12}$ particles for both lithium ions and electrons. The cycling performance is shown in Fig. 5. The capacity fading of the $Li_4Ti_5O_{12}$ powder calcined at 700 °C is faster than those of $Li_4Ti_5O_{12}$ powders calcined at 750 and 800 °C. Furthermore, the initial capacity loss of $Li_4Ti_5O_{12}$ (700 °C) is ca. 8%, while those of $Li_4Ti_5O_{12}$ calcined at 750 and 800 °C are only ca. 5%. It is considered that the crystallization of the $Li_4Ti_5O_{12}$ particles is not very

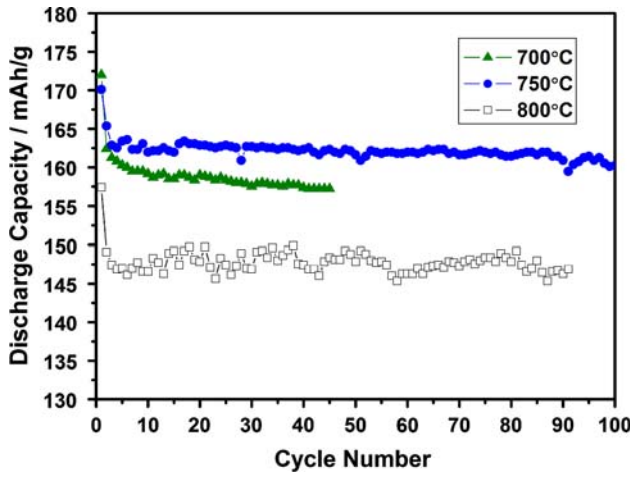

Fig. 5 The cycling performance of the $Li_4Ti_5O_{12}$ powders calcined at various temperatures

good at the temperature of 700 °C. In addition, the capacity fluctuation on cycling is observed in $Li_4Ti_5O_{12}$ (800 °C), which is related to the grain agglomeration at 800 °C [21]. The $Li_4Ti_5O_{12}$ (750 °C) electrode exhibits a high capacity and a good cycling stability; its discharge capacity at the 100th cycle is still 160 mAh/g.

The DC resistance diagram of the $Li_4Ti_5O_{12}$/Li cells as a function of depth-of-discharge (DOD) is shown in Fig. 6. It is evident that the resistance of the $Li_4Ti_5O_{12}$ powders resulting from the three calcination temperatures is very close to each other, about 25 ohm, in the first-half portion of the DOD. After 60% DOD, the resistance of the $Li_4Ti_5O_{12}$/Li cells all increases continuously up to 90% DOD and the peak point of the resistance all appears at 97% DOD, yet with different values, i.e. 1150 ohm (800 °C), 510 ohm (750 °C), and 460 ohm (700 °C), respectively. This difference is believed to be related to the particle size of the $Li_4Ti_5O_{12}$ powders. The resistance related to lithium ion diffusion is a major ingredient for the DC resistance values during the discharge processes [1]. With the progress of lithium intercalation, the shell of $Li_4Ti_5O_{12}$ particles gradually becomes $Li_7Ti_5O_{12}$ structure. The thicker the $Li_7Ti_5O_{12}$ shell in the lithium intercalation process, the harder the lithium ions diffuse into the core of $Li_4Ti_5O_{12}$. This corresponds to the continuous increase of the cell resistance after 60% DOD. Clearly, the particle size plays an important role in the increased DC resistance. The peak value of $Li_4Ti_5O_{12}$ (800 °C) may also explain the capacity of 150 mAh/g previously mentioned.

In general, nanoparticles have good rate performance because of short lithium ion diffusion distance and facile electron transport. The $Li_4Ti_5O_{12}$ powder resulting from the calcinations at 750 °C also exhibits good rate capability. Figure 7 shows initial discharge curves of a

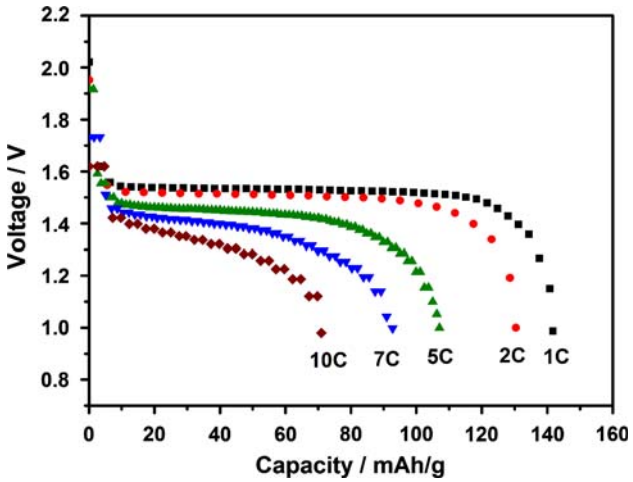

Fig. 7 Discharge curves of an $Li_4Ti_5O_{12}$(750 °C)/Li cell at various current rates. The charge and discharge current densities are equal at each rate

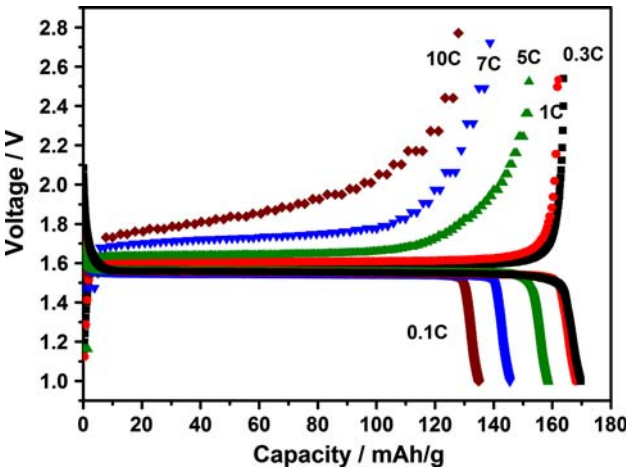

Fig. 9 Rate capability test of the $Li_4Ti_5O_{12}$(750 °C)/Li cell at different rates (0.3C, 1C, 5C, 7C, and 10C). The discharge rate is fixed at 0.1C

$Li_4Ti_5O_{12}$(750 °C)/Li cell at the current rates of 1C, 2C, 5C, 7C, and 10C, respectively. Note that the curves were measured at the same charge and discharge current. At 1C and 2C, the discharge capacity values are ca. 140 and 130 mAh/g, respectively. And both of the discharge voltage plateaus are very close to each other, indicating that the particle size have a slight effect on the rate capability at a medium rate (2C). At 5C, 7C, and up to 10C, the discharge voltage plateau descends more and more, and the discharge capacity drops rapidly.

It is also feasible that a Li-ion cell is charged at a low current density and discharged at a high current density in practical applications. Correspondingly, as an anode material, $Li_4Ti_5O_{12}$ can be discharged at low current density and charged at high current density. Figure 8 shows

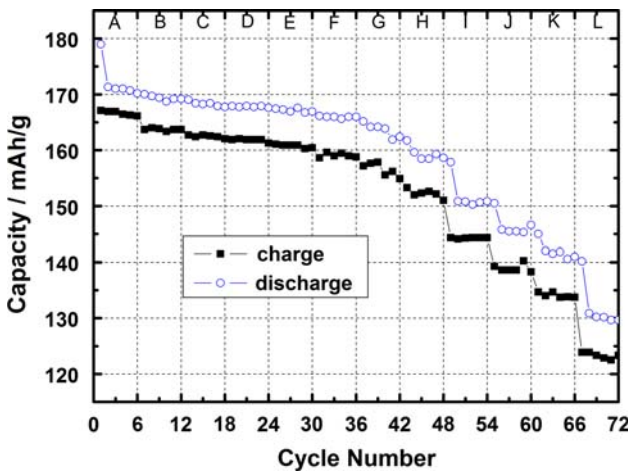

Fig. 8 Capacity performance summary of $Li_4Ti_5O_{12}$(750 °C)/Li cell. Discharge current: 0.1C. Charge current: A: 0.1C; B: 0.3C; C: 0.6C; D: 1C; E: 1.2C; F: 1.5C; G: 2C; H: 3C; I: 5C; J: 7C; K: 8C; L: 10C

capacity performance summary of a $Li_4Ti_5O_{12}$(750 °C)/Li cell at various charge rates with a fixed discharge rate (0.1C, complete discharge in 10 h). The initial discharge capacity at 0.1C is 178 mAh/g, which is slightly above the theoretical capacity (175 mAh/g), suggesting that even the impurity phase (rutile) is intercalated by lithium in the initial discharge process. As the charge current increases, the electrode shows excellent ability of capacity retention. Even at 10C, the charge capacity is 122 mAh/g, which is about 75% of the charge capacity observed at 0.1C.

Figure 9 shows the charge–discharge curves at various charge rates with a fixed discharge rate. Due to the constant discharge rate, the discharge voltage plateau is kept at 1.55 V. The charge voltage plateau varies with different charge rates. From 0.3C to 5C, the difference between the charge voltage plateau and the discharge voltage plateau is small, which represents a fast kinetics of lithium extraction. Furthermore, we anticipate that if the pyrolysis of poly(acrylic acid) takes place in an inert atmosphere, the $Li_4Ti_5O_{12}$ may be coated by a carbon shell, and some Ti^{3+} could be present in the lattice as a dopant, both of which would lead to even better rate capability [22]. This will be subject to our further study.

Conclusions

The nanosized $Li_4Ti_5O_{12}$ powders have been synthesized via a gel polymer route. After calcination at the optimal temperature (750 °C), the powder shows excellent electrochemical performance. After 100 cycles, the capacity of nano-$Li_4Ti_5O_{12}$ is up to 160 mAh/g at C/3 rate. This nano-$Li_4Ti_5O_{12}$ also exhibits a good rate capability with a charge capacity of 122 mAh/g at 10C.

Acknowledgements This study was supported by National Science Foundation of China (grant nos. 50372064 and 20471057). We are also grateful to Dr. Ingo Lieberwirth from Max-Plank Institute at Mainz for FESEM measurement.

References

1. Lu W, Belharouak I, Liu J et al (2007) J Electrochem Soc 154:A114
2. Ma JX, Wang CS, Wroblewski S (2007) J Power Sources 164:849
3. Sorensen EM, Barry SJ, Jung HK et al (2006) Chem Mater 18:482
4. Ariyoshi K, Yamamoto S, Ohzuku T (2003) J Power Sources 119:959
5. Gao J, Ying JR, Jiang CY et al (2007) J Power Sources 166:255
6. Chen CH, Vaughey JT, Jansen AN et al (2001) J Electrochem Soc 148:A102
7. Yao XL, Xie S, Chen CH et al (2005) Electrochim Acta 50:4076
8. Yu Y, Shui JL, Chen CH (2005) Solid State Commun 135:485
9. Scharner S, Weppner W, Schmid-Beurmann P (1999) J Electrochem Soc 146:857
10. Peramunage D, Abraham KM (1998) J Electrochem Soc 145:2615
11. Ferg E, Gummow RJ, Dekock A et al (1994) J Electrochem Soc 141:L147
12. Zaghib K, Armand M, Gauthier M (1998) J Electrochem Soc 145:3135
13. Takai S, Kamata M, Fujine S et al (1999) Solid State Ionics 123:165
14. Ohzuku T, Ueda A, Yamamoto N (1995) J Electrochem Soc 142:1431
15. Bach S, Pereira-Ramos JP, Baffier N (1998) J Mater Chem 8:251
16. Bach S, Pereira-Ramos JP, Baffier N (1999) J Power Sources 82:273
17. Venkateswarlu M, Chen CH, Do JS et al (2005) J Power Sources 146:204
18. Hao YJ, Lai QY, Xu ZH et al (2005) Solid State Ionics 176:1201
19. Shen CM, Zhang XG, Zhou YK et al (2002) Mater Chem Phys 78:437
20. Wang PC, Ding HP, Bark T et al (2007) Electrochim Acta 52:6650
21. Jiang C, Ichihara M, Honma I et al (2007) Electrochim Acta 52:6470
22. Wolfenstine J, Lee U, Allen JL (2006) J Power Sources 154:287